We are IntechOpen, the world's leading publisher of Open Access books Built by scientists, for scientists

4,800
Open access books available

122,000
International authors and editors

135M
Downloads

Our authors are among the

154
Countries delivered to

TOP 1%
most cited scientists

12.2%
Contributors from top 500 universities

CLARIVATE ANALYTICS BOOK CITATION INDEX INDEXED

WEB OF SCIENCE™

Selection of our books indexed in the Book Citation Index in Web of Science™ Core Collection (BKCI)

Interested in publishing with us?
Contact book.department@intechopen.com

Numbers displayed above are based on latest data collected.
For more information visit www.intechopen.com

4

Quantum Manipulations of Single Trapped-Ions Beyond the Lamb-Dicke Limit

M. Zhang and L. F. Wei
Quantum Optoelectronics Laboratory and School of Physics and Technology, Southwest Jiaotong University, Chengdu 610031 China

1. Introduction

An ion can be trapped in a small region in three dimensional space by the electromagnetic trap, and can be effectively manipulated by the applied laser pulses (1; 2; 3). The system of trapped ions driven by laser pulses provides a powerful platform to engineer quantum states (4; 5; 6; 7) and implement quantum information processings (QIPs) (8; 9; 10). Typically, manipulations and detections quantum information can be utilized to test certain fundamental principles (such as EPR and Shrödinger cat "paradox") in quantum mechanics and implement quantum computation, quantum telegraph, and quantum cryptography, etc.(see, e.g., (11; 12; 13; 14)).
Up to now, several kinds of physical systems, e.g., cavity-QEDs (15), superconducting Josephson junctions (16), nuclear magnetic resonances (NMRs) (17), and coupled quantum dots (18), etc., have been proposed to physically implement the QIPs. The system of trapped ions is currently one of the most advanced models for implementing the QIPs, due to its relatively-long coherence time. Indeed, the coherent manipulations up to eight trapped ions had already been experimentally demonstrated (14).
However, most of the quantum manipulations with the trapped cold ions are within the Lamb-Dicke (LD) approximation, e.g., the famous Cirac-Zoller model (8). Such an approximation requires that the coupling between the quantum bit (encoded by two atomic levels of a trapped ion) and the data bus (the collective vibration mode of the ions) should be sufficiently weak. Sometimes, the LD limits could be not rigorously satisfied for typical single trapped-ion system, and thus higher-order powers of the LD parameter must be taken into account (19). Alternatively, the laser-ion interaction beyond the LD approximation might be helpful to reduce the noise in the ion-trap and improve the cooling rate(see, e.g., (20; 21; 22)), and thus could be utilized to high-efficiently realize QIPs.
In this chapter, we summarize our works (23; 24; 25; 26; 27; 28; 29; 30; 31) on how to design proper laser pulses for the desirable quantum-state engineerings with single trapped-ions, including the preparations of various typical quantum states of the data bus and the implementations of quantum logic gates beyond the LD approximation. The chapter is organized as: In Sec. 2 we derivate the dynamical evolutions of a single trapped ion (driven by a classical laser beam) with and beyond the LD approximation. Based on the quantum dynamics beyond the LD approximation, in Sec. 3, we discuss how to use a series of laser pulses to generate various vibrational quantum states of the trapped ion, e.g., coherence states, squeezed coherent states, squeezed odd/even coherent states and squeezed vacuum states, etc. We also present the approach (by properly setting the laser pulses) to realize control-NOT

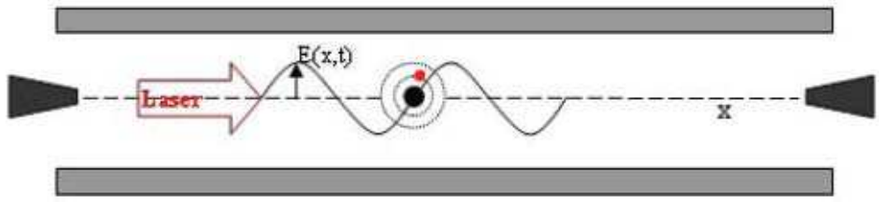

Fig. 1. (Color online) A sketch of an two-level ion trapped in one-dimensional electromagnetic trap (Only the vibrational motion along the x-direction is considered) and driven by a classical laser field propagating along the x direction.

(CNOT) gates (between the internal and external freedoms of a single trapped ion) beyond the LD approximation. In Sec. 4 we give a brief conclusion.

2. Dynamics of single trapped ions driven by laser beams

An electromagnetic-trap can provides a three-dimensional potential to trap an ion (with mass m and charge e). The potential function takes the form (3)

$$U(x,y,z) \approx \frac{1}{2}(\alpha x^2 + \beta y^2 + \gamma z^2), \tag{1}$$

near the trap-center ($x, y, z = 0$), with α, β, and γ bing the related experimental parameters. Therefore, a trapped ion (see, Fig.1) has two degrees of freedom: the vibrational motion around the trap-center and the internal atomic levels of the ion. For simplicity, we consider that the trap provides a pseudopotential whose frequencies satisfy the condition $v_x = v \ll v_y, v_z$. This implies that only the quantized vibrational motion along the x-direction (i.e., the principal axes of the trap) is considered. For the internal degree of freedom of the trapped ion, we consider only two selected levels, e.g., the ground state $|g\rangle$ and excited state $|e\rangle$. The Hamiltonian describing the above two uncoupled degrees of freedom can be written as

$$\hat{H}_0 = \hbar\nu(\hat{a}^\dagger\hat{a} + \frac{1}{2}) + \frac{\hbar}{2}\omega_a\hat{\sigma_z}, \tag{2}$$

where, $\hbar$ is the Planck's constant divided by 2π, $\hat{a}^\dagger$ and $\hat{a}$ are the bosonic creation and annihilation operators of the external vibrational quanta of the cooled ion with frequency ν. $\hat{\sigma_z} = |e\rangle\langle e| - |g\rangle\langle g|$ is the Pauli operator. The transition frequency ω_a is defined by $\omega_a = (E_e - E_g)/\hbar$ with E_g and E_e being the corresponding energies of the two selected levels, respectively.

In order to couple the above two uncoupled degrees of freedom of the trapped ion, we now apply a classical laser beam $E(x,t) = A\cos(k_l x - \omega_l t - \phi_l)$ (propagating along the x direction) to the trapped ion (see Fig. 1), where A, k_l, ω_l, and ϕ_l are its amplitude, wave-vector, frequency, and initial phase, respectively. This yields the laser-ion interaction

$$V = erE(x,t). \tag{3}$$

Certainly, $x = \sqrt{\hbar/2m\nu}(\hat{a} + \hat{a}^\dagger)$ and $r = \langle g|r|e\rangle(|g\rangle\langle e| + |e\rangle\langle g|)$, and thus the above interaction can be further written as

$$\hat{H}_{\rm int} = \frac{\hbar\Omega}{2}\hat{\sigma}_x\left(e^{i\eta(\hat{a}+\hat{a}^\dagger)-i\omega_l t-i\vartheta_l} + e^{-i\eta(\hat{a}+\hat{a}^\dagger)+i\omega_l t+i\vartheta_l}\right), \tag{4}$$

where, $\hat{\sigma}_x = \hat{\sigma}_- + \hat{\sigma}_+$ with $\hat{\sigma}_- = |g\rangle\langle e|$ and $\hat{\sigma}_- = |e\rangle\langle g|$ being the usual raising and lowering operators, respectively. The Rabi frequency $\Omega = eA\langle g|r|e\rangle/\hbar$ describes the strength of coupling between the applied laser field and the trapped ion. Finally, $\eta = k_l\sqrt{\hbar/2m\nu}$ is the so-called LD parameter, which describes the strength of coupling between external and internal degrees of freedom of the trapped ion.
Obviously, the total Hamiltonian, describing the trapped ion driven by a classical laser field, reads

$$\hat{H} = \hat{H}_0 + \hat{H}_{\rm int} = \hbar\nu(\hat{a}^\dagger\hat{a} + \frac{1}{2}) + \frac{\hbar}{2}\omega_a\hat{\sigma}_z + \frac{\hbar\Omega}{2}\hat{\sigma}_x\left(e^{i\eta(\hat{a}+\hat{a}^\dagger)-i\omega_l t-i\vartheta_l} + e^{-i\eta(\hat{a}+\hat{a}^\dagger)+i\omega_l t+i\vartheta_l}\right). \quad (5)$$

This Hamiltonian yields a fundamental dynamics in this chapter for engineering the quantum states of trapped cold ion.

2.1 Within Lamb-Dicke approximation

Up to now, most of the experiments (see, e.g., (10)) for engineering the quantum states of trapped ions are operated under the LD approximation, i.e., supposing the LD parameters are sufficiently small ($\eta \ll 1$) such that one can make the following approximation:

$$e^{\pm i\eta(\hat{a}+\hat{a}^\dagger)} \approx 1 \pm i\eta(\hat{a} + \hat{a}^\dagger). \quad (6)$$

Under such an approximation, the Hamiltonian (5) can be reduced to

$$\hat{H}_{\rm LDA} = \hat{H}_0 + \frac{\hbar\Omega}{2}\hat{\sigma}_x\left[e^{-i\omega_l t-i\vartheta_l} + e^{i\omega_l t+i\vartheta_l} + i\eta e^{-i\omega_l t-i\vartheta_l}(\hat{a}+\hat{a}^\dagger) - i\eta e^{i\omega_l t+i\vartheta_l}(\hat{a}+\hat{a}^\dagger)\right], \quad (7)$$

and can be further written as

$$\begin{aligned}\hat{H}'_{\rm LDA} = {} & \tfrac{\hbar\Omega}{2}\left(e^{-i\omega_a t}\hat{\sigma}_- + \hat{\sigma}_+ e^{i\omega_a t}\right) \\ & \times\left[e^{-i\omega_l t-i\vartheta_l} + e^{i\omega_l t+i\vartheta_l} + i\eta e^{-i\omega_l t-i\vartheta_l}(e^{-i\nu t}\hat{a} + e^{i\nu t}\hat{a}^\dagger) - i\eta e^{i\omega_l t+i\vartheta_l}(e^{-i\nu t}\hat{a} + e^{i\nu t}\hat{a}^\dagger)\right]\end{aligned} \quad (8)$$

in the interaction picture defined by the unity operator $\hat{U} = \exp(-it\hat{H}_0/\hbar)$. Note that, to obtain the interacting Hamiltonian (8), we have used the following relations

$$\begin{cases} e^{-i\alpha\hat{\sigma}_z}\hat{\sigma}_z e^{i\alpha\hat{\sigma}_z} = \hat{\sigma}_z \\ e^{-i\alpha\hat{\sigma}_z}\hat{\sigma}_+ e^{i\alpha\hat{\sigma}_z} = e^{i2\alpha}\hat{\sigma}_+ \\ e^{-i\alpha\hat{\sigma}_z}\hat{\sigma}_- e^{i\alpha\hat{\sigma}_z} = e^{-i2\alpha}\hat{\sigma}_- \\ e^{-i\alpha\hat{a}^\dagger\hat{a}} f(\hat{a}^\dagger,\hat{a}) e^{i\alpha\hat{a}^\dagger\hat{a}} = f(e^{i\alpha}\hat{a}^\dagger, e^{-i\alpha}\hat{a}). \end{cases} \quad (9)$$

Above, α is an arbitrary parameter and $f(\hat{a}^\dagger,\hat{a})$ is an arbitrary function of operators $\hat{a}^\dagger$ and $\hat{a}$. Now, we assume that the frequencies of the applied laser fields are set as $\omega_l = \omega_0 + K\nu$, with $K = 0, \pm 1$ corresponding to the usual resonance ($K = 0$), the first blue- ($K = 1$), and red- ($K = 1$) sideband excitations (4), respectively. As a consequence, the Hamiltonian (8) can be specifically simplified to (30)

$$\hat{H}^0_{\rm LDA} = \frac{\hbar\Omega}{2}\left(e^{i\vartheta_l}\hat{\sigma}_- + e^{-i\vartheta_l}\hat{\sigma}_+\right) \qquad \text{for } K = 0, \quad (10)$$

$$\hat{H}^{\rm r}_{\rm LDA} = \frac{\hbar\Omega}{2} i\eta\left(e^{-i\vartheta_l}\hat{\sigma}_+\hat{a} - e^{i\vartheta_l}\hat{\sigma}_-\hat{a}^\dagger\right) \quad \text{for } K = -1, \quad (11)$$

$$\hat{H}^{\rm b}_{\rm LDA} = \frac{\hbar\Omega}{2} i\eta \left(e^{-i\vartheta_l} \hat{\sigma}_+ \hat{a}^\dagger - e^{i\vartheta_l} \hat{\sigma}_- \hat{a} \right) \quad \text{for } K = -1, \tag{12}$$

under the rotating-wave approximation (i.e., neglected the rapidly-oscillating terms in Eq. (8)). Obviously, the Hamiltonian $\hat{H}^0_{\rm LDA}$ describes a Rabi oscillation and corresponds to a one-qubit operation, and Hamiltonians $\hat{H}^{\rm r}_{\rm LDA}$ and $\hat{H}^{\rm b}_{\rm LDA}$ correspond to the Jaynes-Cummings (JC) model (JCM) and anti-JCM (4), respectively. It is well-known that the JCM describes the basic interaction of a two-level atom and a quantized electromagnetic field (15). Here, the quantized electromagnetic field is replaced by the quantized vibration of the trapped ion, and thus the entanglement between the external motional states and the internal atomic states of the ions can be induced. Certainly, these JC interactions take the central role in the current trap-ion experiments for implementing the QIPs (10).

2.2 Beyond the LD approximation

In principle, quantum motion of the trapped ions beyond the usual LD limit ($\eta \ll 1$) is also possible. Utilizing the laser-ion interaction outside the LD regime might be helpful to reduce the noise in the ion-trap and improve the cooling rate, and thus could be utilized to efficiently realize QIPs. Indeed, several approaches have been proposed to coherently operate trapped ions beyond the LD limit (see, e.g., (19)).

Because $[\hat{a}, \hat{a}^\dagger] = 1$, the term $\exp[\pm i\eta(\hat{a} + \hat{a}^\dagger)]$ in Eq. (5) can be expanded as

$$e^{\pm i\eta(\hat{a}+\hat{a}^\dagger)} = e^{-\eta^2/2} e^{\pm i\eta\hat{a}^\dagger} e^{\pm i\eta\hat{a}} = e^{-\eta^2/2} \sum_{n,m}^{\infty} \frac{(\pm i\eta\hat{a}^\dagger)^n (\pm i\eta\hat{a})^m}{n!m!}. \tag{13}$$

Comparing to the expansion Eq. (6), the above expansion is exactly, and the LD parameter can be taken as an arbitrary value. With the help of relation (9) and (13), the Hamiltonian (5) can be written as:

$$\begin{aligned} \hat{H}'_{\rm NLDA} = \tfrac{\hbar\Omega}{2}\hat{\sigma}_+ \Bigg(& e^{i(\omega_a+\omega_l)t} e^{i\vartheta_l} e^{-\eta^2/2} \textstyle\sum_{n,m}^{\infty} \frac{(-i\eta\hat{a}^\dagger e^{ivt})^n (-i\eta\hat{a}e^{-ivt})^m}{n!m!} \\ & + e^{i(\omega_a-\omega_l)t} e^{-i\vartheta_l} e^{-\eta^2/2} \textstyle\sum_{n,m}^{\infty} \frac{(i\eta\hat{a}^\dagger e^{ivt})^n (i\eta\hat{a}e^{-ivt})^m}{n!m!} \Bigg) + H.c \end{aligned} \tag{14}$$

in the interaction picture defined by unity operator $\hat{U} = \exp(-it\hat{H}_0/\hbar)$.

For the so-called sideband excitations $\omega_l = \omega_0 + K\nu$ with K being arbitrary integer, the above Hamiltonian can be reduced to (23; 26)

$$\hat{H}^r_{\rm NLDA} = \frac{\hbar\Omega}{2} e^{-\eta^2/2} \left[e^{-i\vartheta_l} (i\eta)^k \hat{\sigma}_+ \sum_{j=0}^{\infty} \frac{(i\eta)^{2j} (\hat{a}^\dagger)^j \hat{a}^{j+k}}{j!(j+k)!} + H.c \right] \quad \text{for} \quad K \leq 0 \tag{15}$$

$$\hat{H}^b_{\rm NLDA} = \frac{\hbar\Omega}{2} e^{-\eta^2/2} \left[e^{-i\vartheta_l} (i\eta)^k \hat{\sigma}_+ \sum_{j=0}^{\infty} \frac{(i\eta)^{2j} (\hat{a}^\dagger)^{j+k} \hat{a}^j}{j!(j+k)!} + H.c \right] \quad \text{for} \quad K \geq 0 \tag{16}$$

under the rotating wave approximation. Above, $K = 0$, $K < 0$, and $K > 0$ correspond to the resonance, the kth blue-, and red-sideband excitations (with $k = |K|$), respectively. Comparing with Hamiltonian (10)-(12) with LD approximation, the above Hamiltonian (without performing the LD approximation) can describes various multi-phonon transitions (i.e., $k > 1$) (19). This is due to the contribution from the high order effects of LD parameter.

2.3 Time evolutions of quantum states

The time evolution of the system governed by the above Hamiltonian can be solved by the time-evolution operator $\hat{T} = \exp(-it\hat{H}/\hbar)$, with $\hat{H}$ taking $\hat{H}^0_{\rm LDA}$, $\hat{H}^r_{\rm LDA}$, $\hat{H}^b_{\rm LDA}$, $\hat{H}^r_{\rm NLDA}$, and $\hat{H}^b_{\rm NLDA}$, respectively. For an arbitrary initial state $|\varphi(0)\rangle$, the evolving state at time t reads

$$|\varphi(t)\rangle = \hat{T}|\varphi(0)\rangle = \sum_{n=0}^{\infty} \frac{1}{n!}\left(\frac{-it}{\hbar}\right)^n \hat{H}^n |\varphi(0)\rangle. \tag{17}$$

Typically, if the external vibrational state of the ion is initially in a Fock state $|m\rangle$ and the internal atomic state is initially in the atomic ground sate $|g\rangle$ or excited one $|e\rangle$, then the above dynamical evolutions can be summarized as follows (23; 26):
i) For the resonance or red-sideband excitations $K \leq 0$:

$$\begin{cases} |m\rangle|g\rangle \longrightarrow |m\rangle|g\rangle, \; m < k, \\ |m\rangle|g\rangle \longrightarrow \cos(\Omega_{m-k,k}t)|m\rangle|g\rangle + i^{k-1}e^{-i\vartheta_l}\sin(\Omega_{m-k,k}t)|m-k\rangle|e\rangle; \; m \geq k, \\ |m\rangle|e\rangle \longrightarrow \cos(\Omega_{m,k}t)|m\rangle|e\rangle - (-i)^{k-1}e^{i\vartheta_l}\sin(\Omega_{m,k}t)|m+k\rangle|g\rangle \end{cases} \tag{18}$$

ii) For the resonance or blue-sideband excitations $K \geq 0$:

$$\begin{cases} |m\rangle|g\rangle \longrightarrow \cos(\Omega_{m,k}t)|m\rangle|g\rangle + i^{k-1}e^{-i\vartheta_l}\sin(\Omega_{m,k}t)|m+k\rangle|e\rangle, \\ |m\rangle|e\rangle \longrightarrow |m\rangle|e\rangle, \; m < k, \\ |m\rangle|e\rangle \longrightarrow \cos(\Omega_{m-k,k}t)|m\rangle|e\rangle - (-i)^{k-1}e^{i\vartheta_l}\sin(\Omega_{m-k,k}t)|m-k\rangle|g\rangle, \; m \geq k. \end{cases} \tag{19}$$

The so-called effective Rabi frequency introduced above reads

$$\Omega_{m,k} = \begin{cases} \Omega^L_{m,k} = \frac{\Omega}{2}\eta^k\sqrt{\frac{(m+k)!}{m!}}, \quad k = 0, 1, \\ \\ \Omega^N_{m,k} = \frac{\Omega}{2}\eta^k e^{-\eta^2/2}\sqrt{\frac{(m+k)!}{m!}}\sum_{j=0}^{m}\frac{(i\eta)^{2j}m!}{(j+k)!j!(m-j)!}, \quad k = 0, 1, 2, 3, \ldots. \end{cases} \tag{20}$$

The above derivations show that the dynamics either within or beyond the LD approximation has the same form (see, Eqs. (18) and (19)), only the differences between them is represented by the specifical Rabi frequencies $\Omega^L_{m,k}$ and $\Omega^N_{m,k}$. Certainly, the dynamical evolutions without LD approximation are more closed to the practical situations of the physical processes. Furthermore, comparing to dynamics with LD approximation (where $k = 0, 1$), the dynamics without LD approximation (where $k = 0, 1, 2, 3, ...$) can describes various multi-phonon transitions.
Certainly, when the LD parameters are sufficiently small, i.e., $\eta \ll 1$, the rate

$$\gamma = \frac{\Omega^L_{m,k}}{\Omega^N_{m,k}} = \frac{e^{\eta^2/2}}{\sum_{j=0}^{m}\frac{(i\eta)^{2j}m!}{(j+k)!j!(m-j)!}} \sim 1, \tag{21}$$

and thus the dynamics within LD approximation works well. Whereas, if the LD parameter are sufficiently large, the quantum dynamics beyond the LD limit must be considered.

3. Quantum-state engineerings beyond the LD limit

3.1 Preparations of various motional states of the single ions

The engineering of quantum states has attracted considerable attention in last two decades. This is in order to test fundamental quantum concepts such as non-locality, and for implementing various potential applications, including sensitive detections and quantum information processings. Laser-cooled single trapped ions are the good candidates for various quantum-state engineering processes due to their relatively-long decoherence times. Indeed, various engineered quantum states of trapped cold ions have been studied. The thermal, Fock, coherent, squeezed, and arbitrary quantum superposition states of motion of a harmonically bound ion have been investigated (4; 5; 6; 7). However, most of the related experiments are operated under the LD approximation. In this section we study the engineerings of various typical vibrational states of single trapped ions beyond the LD limit.

There are serval typical quantum states in quantum optics: coherence states, odd/even coherent states and squeezed states, etc.. They might show highly nonclassical properties, such as squeezing, anti-bunching and sub-Poissonian photon statistics. In the Fock space, coherence state $|\alpha\rangle$ can be regarded as a displaced vacuum state, i.e.,

$$|\alpha\rangle = D(\alpha)|0\rangle = e^{-|\alpha|^2/2}\sum_{n=0}^{\infty}\frac{\alpha^n}{\sqrt{n!}}|n\rangle, \tag{22}$$

where $D(\alpha) = \exp(\alpha\hat{a}^{\dagger} - \alpha^*\hat{a})$ is the so-called displace operator, with α being a complex parameter and describing the strength of displace. Similarly, the squeezed states $|\psi_s\rangle$ are generated by applying the squeeze operator to a quantum state

$$|\psi_s\rangle = \hat{S}(\xi)|\psi\rangle, \tag{23}$$

where $\hat{S} = \exp(\xi^*\hat{a}^2/2 - \xi\hat{a}^{\dagger 2}/2)$, and ξ is a complex parameter describing the strength of the squeezes. On the other hand, the odd/even coherent states are the superposed states of two coherent states with different phases

$$|\alpha_o\rangle = C_o(|\alpha\rangle - |-\alpha\rangle), \tag{24}$$

$$|\alpha_e\rangle = C_e(|\alpha\rangle + |-\alpha\rangle). \tag{25}$$

Above, $C_o = [2 - 2\exp(-2|\alpha|^2)]^{-1/2}$ and $C_e = [2 + 2\exp(-2|\alpha|^2)]^{-1/2}$ are the normalized coefficients.

According to the above definitions: Eqs. (22)-(25), one can obtain the squeezed coherent state:

$$|\alpha_s\rangle = \hat{S}(\xi)|\alpha\rangle = \sum_{n=0}^{\infty} G_n(\alpha,\xi)|n\rangle, \tag{26}$$

squeezed vacuum state:

$$|0_s\rangle = \hat{S}(\xi)|\alpha = 0\rangle = \sum_{n=0}^{\infty} G_n(0,\xi)|n\rangle, \tag{27}$$

squeezed odd state:

$$|\alpha_{o,s}\rangle = \hat{S}(\xi)|\alpha_o\rangle = \sum_{n=0}^{\infty} O_n(\alpha,\xi)|n\rangle, \tag{28}$$

and squeezed even state:

$$|\alpha_{e,s}\rangle = \hat{S}(\xi)|\alpha_e\rangle = \sum_{n=0}^{\infty} E_n(\alpha,\xi)|n\rangle. \tag{29}$$

respectively. Above,

$$G_n(\alpha,\xi) = \frac{1}{\sqrt{\cosh(r)n!}}\left(\frac{e^{i\theta}\sinh(r)}{2\cosh(r)}\right)^{n/2}\exp[\frac{e^{-i\theta}\sinh(r)\alpha^2}{2\cosh(r)} - \frac{|\alpha|^2}{2}]H_n(\frac{\alpha}{\sqrt{2e^{i\theta}\sinh(r)\cosh(r)}}). \tag{30}$$

with $\xi = r\exp(i\theta)$, and $H_n(x)$ being the hermitian polynomials. Finally,

$$O_n(\alpha,\xi) = C_o\left(G_n(\alpha,\xi) - G_n(-\alpha,\xi)\right) \tag{31}$$

and

$$E_n(\alpha,\xi) = C_e\left(G_n(\alpha,\xi) + G_n(-\alpha,\xi)\right). \tag{32}$$

Based on the quantum dynamics of laser-ion interaction beyond the LD limit, in what follows we discuss how to use a series of laser pulses to generate the above vibrational quantum states of the trapped ions. Assuming the trapped ion is initialized in the state $|0\rangle|g\rangle$, to generate the desirable quantum states we use the following sequential laser pulses to drive the trapped ion:

1) Firstly, a pulse with frequency $\omega_l = \omega_a$, initial phase ϑ_1, and duration t_1 is applied on the trapped ion to yield the evolution:

$$|0\rangle|g\rangle \to |\psi_1\rangle = \cos(\Omega_{0,0}t_1)|0\rangle|g\rangle + i^{-1}e^{-i\vartheta_1}\sin(\Omega_{0,0}t_1)|0\rangle|e\rangle \tag{33}$$

2) Secondly, a pulse with frequency $\omega_l = \omega_a - \nu$, initial phase ϑ_2, and duration t_2 is applied on the ion to generate:

$$\begin{aligned}|\psi_1\rangle \to |\psi_2\rangle = &\cos(\Omega_{0,0}t_1)|0\rangle|g\rangle + ie^{i(\vartheta_2-\vartheta_1)}\sin(\Omega_{0,0}t_1)\sin(\Omega_{0,1}t_2)|1\rangle|g\rangle \\ &+i^{-1}e^{-i\vartheta_1}\sin(\Omega_{0,0}t_1)\cos(\Omega_{0,1}t_2)|0\rangle|e\rangle\end{aligned} \tag{34}$$

3) Thirdly, a pulse with frequency $\omega_l = \omega_a - 2\nu$, initial phase ϑ_3, and duration t_3 is applied on the ion to generate:

$$\begin{aligned}|\psi_2\rangle \to |\psi_3\rangle = &\cos(\Omega_{0,0}t_1)|0\rangle|g\rangle + ie^{i(\vartheta_2-\vartheta_1)}\sin(\Omega_{0,0}t_1)\sin(\Omega_{0,1}t_2)|1\rangle|g\rangle \\ &+e^{i(\vartheta_3-\vartheta_1)}\sin(\Omega_{0,0}t_1)\cos(\Omega_{0,1}t_2)\sin(\Omega_{0,2}t_3)|2\rangle|g\rangle \\ &+i^{-1}e^{-i\vartheta_1}\sin(\Omega_{0,0}t_1)\cos(\Omega_{0,1}t_2)\cos(\Omega_{0,2}t_3)|0\rangle|e\rangle\end{aligned} \tag{35}$$

4) Successively, after the Nth pulse (with frequency $\omega_l = \omega_a - (N-1)\nu$, initial phase ϑ_N, and duration t_N) is applied on the ion, we have the following superposition state:

$$|\psi_{N-1}\rangle \to |\psi_N\rangle = \sum_{n=0}^{N-1} C_n|n\rangle|g\rangle + B_N|0\rangle|e\rangle \tag{36}$$

with

$$C_n = \begin{cases} \cos(\Omega_{0,0}t_1), & n=0, \\ ie^{i(\vartheta_2-\vartheta_1)}\sin(\Omega_{0,0}t_1)\sin(\Omega_{0,1}t_2), & n=1, \\ (-1)^{n-1}i^n e^{i(\vartheta_{n+1}-\vartheta_1)}\sin(\Omega_{0,0}t_1)\sin(\Omega_{0,n}t_{n+1})\prod_{j=2}^{n}\cos(\Omega_{0,j-1}t_j), & n>1, \end{cases} \tag{37}$$

and

$$B_N = \begin{cases} i^{-1}e^{-i\vartheta_1}\sin(\Omega_{0,0}t_1), & N=1, \\ i^{-1}e^{-i\vartheta_1}\sin(\Omega_{0,0}t_1)\prod_{j=2}^{N}\cos(\Omega_{0,j-1}t_j), & N>1 \end{cases} \tag{38}$$

If the duration of Nth ($N > 1$) laser pulse is set to satisfy the condition $\cos(\Omega_{0,N-1}t_N) = 0$, then $B_N = 0$. This implies that the internal state of the trapped ion is returned to the ground state $|g\rangle$ and its external vibration is prepared on the superposition state $|\psi_N^{\rm ex}\rangle = \sum_{n=0}^{N-1} C_n|n\rangle$. Because the durations t_N and initial phases ϑ_N are experimentally controllable, we can set $C_n = G_n(\alpha,\xi)$, $O_n(\alpha,\xi)$, or $E_n(\alpha,\xi)$ with $n \leq N-2$ by selecting the proper t_N and ϑ_N. As a consequence, we have the vibrational superposition state:

$$|\psi_N^G\rangle = \sum_{n=0}^{N-2} G_n(\alpha,\xi)|n\rangle + C_{N-1}^G|n-1\rangle, \tag{39}$$

$$|\psi_N^O\rangle = \sum_{n=0}^{N-2} O_n(\alpha,\xi)|n\rangle + C_{N-1}^O|n-1\rangle, \tag{40}$$

$$|\psi_N^E\rangle = \sum_{n=0}^{N-2} E_n(\alpha,\xi)|n\rangle + C_{N-1}^E|n-1\rangle, \tag{41}$$

and

$$|C_{N-1}^G|^2 = 1 - \sum_{n=0}^{N-2}|G_n(\alpha,\xi)|^2, \tag{42}$$

$$|C_{N-1}^O|^2 = 1 - \sum_{n=0}^{N-2}|O_n(\alpha,\xi)|^2, \tag{43}$$

$$|C_{N-1}^E|^2 = 1 - \sum_{n=0}^{N-2}|E_n(\alpha,\xi)|^2. \tag{44}$$

If the number of the laser pulses, i.e., N, are sufficiently large, the superposition states (39), (40), and (41) can well approach the desirable squeezed coherent state, squeezed odd and even coherent states, respectively. Specifically, when $\xi = 0$, the usual coherent state, odd/even coherent states are generated.

Table 1 presents some numerical results for generating squeezed coherent states, where the typical values of parameters α and ξ, e.g., $\alpha = 2$ and $\xi = 0.5$, are considered. When $\alpha = 0$, the squeezed coherent states correspond to the squeezed vacuum states. On the other hand, some results for generating squeezed odd/even coherent states are shown in table 2, and

α	ξ	N	$\Omega t_1(\vartheta_1)$	$\Omega t_2(\vartheta_2)$	$\Omega t_3(\vartheta_3)$	$\Omega t_4(\vartheta_4)$	$\Omega t_5(\vartheta_5)$	$\Omega t_6(\vartheta_6)$	F
0	0.5	5	0.7080(0)	0(0)	53.9174(π)	0(0)	4065.1(π)		0.9983
0	0.8	5	1.0859(0)	0(0)	43.9507(π)	0(0)	4065.1(π)		0.9816
1	0.0	5	1.8966(0)	7.1614($3\pi/2$)	46.0741(0)	343.5682($\pi/2$)	4065.1(0)		0.9981
2	0.5	5	2.5666(0)	5.3267($3\pi/2$)	43.7265(0)	371.8479($\pi/2$)	4065.1(π)		0.9882
2	0.5	6	2.5666(0)	5.3267($3\pi/2$)	43.7265(0)	371.8479($\pi/2$)	1826.3(π)	3635.9(0)	0.9910
2	0.8	6	2.2975(0)	6.8280($3\pi/2$)	43.9627(0)	59.8973($\pi/2$)	1877.7(π)	3635.9(0)	0.9821

Table 1. Parameters for generating squeezed coherent states, with the typical $\eta = 0.25$

odd/even	α	ξ	N	$\Omega t_1(\vartheta_1)$	$\Omega t_2(\vartheta_2)$	$\Omega t_3(\vartheta_3)$	$\Omega t_4(\vartheta_4)$	$\Omega t_5(\vartheta_5)$	$\Omega t_6(\vartheta_6)$	F
odd	1	0.0	5	3.2413(0)	9.6943($3\pi/2$)	0(0)	436.5962($\pi/2$)	4065.1(0)		0.9927
odd	2	0.5	6	3.2413(0)	7.7328($3\pi/2$)	0(0)	438.6774($\pi/2$)	0(0)	3635.9(0)	0.9974
odd	2	0.8	6	3.2413(0)	9.9520($3\pi/2$)	0(0)	85.3471($\pi/2$)	0(0)	3635.9(0)	0.9763
even	1	0.0	5	1.3106(0)	0(0)	59.9889(0)	0(0)	4065.1(0)		0.9995
even	2	0.5	5	2.2687(0)	0(0)	61.3354(0)	0(0)	4065.1(0)		0.9870
even	2	0.8	5	1.8498(0)	0(0)	51.1086(0)	0(0)	4065.1(0)		0.9900

Table 2. Parameters for generating squeezed odd/even coherent states, with the typical $\eta = 0.25$

where, $\xi = 0$ corresponds to the usual odd/even coherent states. By properly setting the durations t_N and phases ϑ_N of each laser pulse, the desirable squeezed states of the trapped ion could be generated with high fidelities (e.g., 99%), via few steps of laser pulse operations (e.g., $N = 6$). Here, the fidelities $F = \langle\psi_{\text{generated}}|\psi_{\text{expected}}\rangle$ are defined by the overlaps between the generated quantum states $|\psi_{\text{generated}}\rangle$ (being $|\psi_N^G\rangle$, $|\psi_N^O\rangle$, or $|\psi_N^E\rangle$) and the expected states $|\psi_{\text{expected}}\rangle$.

Above, the frequencies, durations, phases, and powers of the laser pulses should be set sufficiently exact for realizing the high fidelity quantum state operations. In fact, it is not difficult to generate the desired laser pulse with current experimental technology. It has been experimentally demonstrated that, a Fock state up to $|n = 16\rangle$ can be generated from the vibrational ground state $|0\rangle$, by sequentially applying laser pulses (with exact frequencies, durations, and phases, etc.) to the trapped ion (2; 4). This means that here the generation of the superposed Fock states, being coherent state, even/odd coherent states, or squeezed quantum states, etc., is also experimentally realizability.

On the other hand, the generation of the superposed Fock states is limited in practice by the existing decays of the vibrational and atomic states. Experimentally, the lifetime of the atomic excited states $|e\rangle$ reaches 1s and the coherence superposition of vibrational states $|0\rangle$ and $|1\rangle$ can be maintained for up to 1ms (32; 33). Therefore, roughly say, preparing the above superposed vibrational Fock states is experimentally possible, as the durations of quantum operation are sufficiently short, e.g., < 0.1 ms. To realize a short operation time, the Rabi frequencies Ω (describing the strength of the laser-ion interaction) should be set sufficiently large, e.g., when $\Omega = 10^5$ kHz, the total duration $t = t_1 + t_2 + t_3 \approx 0.04$ ms for generating squeezed vacuum state (see, table 1).

Certainly, by increasing the Rabi frequency $\Omega \propto \sqrt{P}$ via enhancing the power P of the applied laser beams, the operational durations can be further shorten. For example, if the Rabi frequency Ω increases ten times, then the total durations presented above for generating the desired quantum states could be shortened ten times. Therefore, the desired quantum states could be realized more efficiently. Indeed, the power of the laser applied to drive the trapped cold ion is generally controllable, e.g., it can be adjusted in the range from a few microwatts to a few hundred milliwatts (32).

3.2 Implementations of fundamental quantum logic gates

There is much interest in constructing quantum computer, which uses the principles of quantum mechanics to solve certain problems that could never been solved by any classical computer. An quantum computer is made up of many interacting units called quantum bits or qubits, which usually consist of two quantum states, e.g., $|0\rangle$ and $|1\rangle$. Unlike the classical

bit, which hold either 0 or 1, qubit can hold $|0\rangle$, $|1\rangle$, or any quantum superposition of these states. Therefor, an quantum computer can solve certain problems much faster than any of our current classical computers, such as factoring large numbers (34) and searching large databases (35).

It has been shown that a quantum computer can be built using a series of one-qubit operations and two-qubit controlled-NOT (CNOT) gates, because any computation can be decomposed into a sequence of these basic logic operations (36; 37; 38). Therefore, a precondition work for realizing quantum computation is to effectively implement these fundamental logic gates. Indeed, since the first experiment of demonstrating quantum gates (10), with a single trapped cold ion, much attention has been paid to implement the elementary quantum gates in the systems of trapped cold ions, due to its relatively-long coherence times. However, most of previous approaches are work in LD limit. Following, we study the generations of CNOT gates beyond the LD limit.

A CNOT gate of a single trapped ion can be expressed as (10)

$$\begin{array}{cc} \text{Input state} & \text{Output state} \\ |0\rangle|g\rangle \longrightarrow & |0\rangle|g\rangle \\ |0\rangle|e\rangle \longrightarrow & |0\rangle|g\rangle \\ |1\rangle|g\rangle \longrightarrow & |1\rangle|e\rangle \\ |1\rangle|e\rangle \longrightarrow & |1\rangle|g\rangle \end{array} \tag{45}$$

Above, two lowest occupation number states $|0\rangle$ and $|1\rangle$ of the external vibration of the ion encode the control qubit and selected two atomic levels $|g\rangle$ and $|e\rangle$ of the internal degree of freedom of the ion define the target qubit. It is seen that, if the control qubit is in $|0\rangle$ the target qubit unchanged, whereas, if the control qubit is in $|1\rangle$ the target qubit is changed: $|g\rangle \rightleftarrows |e\rangle$, and thus a CNOT operation is implemented.

Without preforming the LD approximation, the CNOT gate could be implemented by sequentially applying three pulses of the laser beams:

1) A resonance pulse with frequency $\omega_l = \omega_a$, initial phase ϑ_1, and the duration t_1 is applied to implement the operation:

$$\begin{array}{l} |0\rangle|g\rangle \longrightarrow |\psi_a^{(1)}\rangle = \alpha_{11}^{(1)}|0\rangle|g\rangle + \alpha_{12}^{(1)}|0\rangle|e\rangle \\ |0\rangle|e\rangle \longrightarrow |\psi_b^{(1)}\rangle = \alpha_{21}^{(1)}|0\rangle|e\rangle + \alpha_{22}^{(1)}|0\rangle|g\rangle \\ |1\rangle|g\rangle \longrightarrow |\psi_c^{(1)}\rangle = \alpha_{31}^{(1)}|1\rangle|g\rangle + \alpha_{32}^{(1)}|1\rangle|e\rangle \\ |1\rangle|e\rangle \longrightarrow |\psi_d^{(1)}\rangle = \alpha_{41}^{(1)}|1\rangle|e\rangle + \alpha_{42}^{(1)}|1\rangle|g\rangle \end{array} \tag{46}$$

2) A red sideband pulse with the frequency $\omega_l = \omega_a - \nu$, initial phase ϑ_2, and duration t_2 is applied to implement the evolution

$$\begin{array}{l} |\psi_a^{(1)}\rangle \longrightarrow |\psi_a^{(2)}\rangle = \alpha_{11}^{(2)}|0\rangle|g\rangle + \alpha_{12}^{(2)}|0\rangle|e\rangle + \alpha_{13}^{(2)}|0\rangle|g\rangle \\ |\psi_b^{(1)}\rangle \longrightarrow |\psi_b^{(2)}\rangle = \alpha_{21}^{(2)}|0\rangle|g\rangle + \alpha_{22}^{(2)}|0\rangle|e\rangle + \alpha_{23}^{(2)}|1\rangle|g\rangle \\ |\psi_c^{(1)}\rangle \longrightarrow |\psi_c^{(2)}\rangle = \alpha_{31}^{(2)}|0\rangle|e\rangle + \alpha_{32}^{(2)}|1\rangle|g\rangle + \alpha_{33}^{(2)}|1\rangle|e\rangle + \alpha_{34}^{(2)}|2\rangle|g\rangle \\ |\psi_d^{(1)}\rangle \longrightarrow |\psi_d^{(2)}\rangle = \alpha_{41}^{(2)}|0\rangle|e\rangle + \alpha_{42}^{(2)}|1\rangle|g\rangle + \alpha_{43}^{(2)}|1\rangle|e\rangle + \alpha_{44}^{(2)}|2\rangle|g\rangle \end{array} \tag{47}$$

3) A resonance pulse with the initial phase $\vartheta_3 = -\pi/2$ and duration $t_3 = \pi/(4\Omega_{0,0}^L)$ is again applied to implement the following operation

$$\begin{array}{l}
|\psi_a^{(2)}\rangle \longrightarrow |\psi_a^{(3)}\rangle = \alpha_{11}^{(3)}|0\rangle|g\rangle + \alpha_{12}^{(3)}|0\rangle|e\rangle + \alpha_{13}^{(3)}|1\rangle|g\rangle + \alpha_{14}^{(3)}|1\rangle|e\rangle \\
|\psi_b^{(2)}\rangle \longrightarrow |\psi_b^{(3)}\rangle = \alpha_{21}^{(3)}|0\rangle|g\rangle + \alpha_{22}^{(3)}|0\rangle|e\rangle + \alpha_{23}^{(3)}|1\rangle|g\rangle + \alpha_{24}^{(3)}|1\rangle|e\rangle \\
|\psi_c^{(2)}\rangle \longrightarrow |\psi_c^{(3)}\rangle = \alpha_{31}^{(3)}|0\rangle|g\rangle + \alpha_{32}^{(3)}|0\rangle|e\rangle + \alpha_{33}^{(3)}|1\rangle|g\rangle + \alpha_{34}^{(3)}|1\rangle|e\rangle + \alpha_{35}^{(3)}|2\rangle|g\rangle + \alpha_{36}^{(3)}|2\rangle|e\rangle \\
|\psi_d^{(2)}\rangle \longrightarrow |\psi_d^{(3)}\rangle = \alpha_{41}^{(3)}|0\rangle|g\rangle + \alpha_{42}^{(3)}|0\rangle|e\rangle + \alpha_{43}^{(3)}|1\rangle|g\rangle + \alpha_{44}^{(3)}|1\rangle|e\rangle + \alpha_{45}^{(3)}|2\rangle|g\rangle + \alpha_{46}^{(3)}|2\rangle|e\rangle
\end{array} \tag{48}$$

Above, the coefficients $\alpha_{11}^{(1)}$, $\alpha_{12}^{(1)}$, and $\alpha_{13}^{(1)}$ et. al. are derived in APPENDIX A, basing on the dynamical evolution Eqs. (18) and (19).
With the above sequential three operations, the system undergoes the following evolution:

$$\begin{array}{ll}
\text{Input state} & \text{Output state} \\
|0\rangle|g\rangle \longrightarrow |\psi_a^{(1)}\rangle \longrightarrow |\psi_a^{(2)}\rangle \longrightarrow |\psi_a^{(3)}\rangle & \\
|0\rangle|e\rangle \longrightarrow |\psi_b^{(1)}\rangle \longrightarrow |\psi_b^{(2)}\rangle \longrightarrow |\psi_b^{(3)}\rangle & \\
|1\rangle|g\rangle \longrightarrow |\psi_c^{(1)}\rangle \longrightarrow |\psi_c^{(2)}\rangle \longrightarrow |\psi_c^{(3)}\rangle & \\
|1\rangle|e\rangle \longrightarrow |\psi_d^{(1)}\rangle \longrightarrow |\psi_d^{(2)}\rangle \longrightarrow |\psi_d^{(3)}\rangle &
\end{array} \tag{49}$$

Obviously, if $|\psi_a^{(3)}\rangle = |0\rangle|g\rangle$, $|\psi_b^{(3)}\rangle = |0\rangle|e\rangle$, $|\psi_c^{(3)}\rangle = |1\rangle|e\rangle$, and $|\psi_d^{(3)}\rangle = |1\rangle|g\rangle$, the CNOT gate (45) is realized. This means that the coefficients should satisfy the condition (see, Eq. (48)):

$$\alpha_{11}^{(3)} = \alpha_{22}^{(3)} = \alpha_{34}^{(3)} = \alpha_{43}^{(3)} = 1, \tag{50}$$

i.e.,(see, APPENDIX A):

$$\left\{\begin{array}{l}
1 = \cos(\Omega_{0,0}t_1)\cos(\Omega_{0,0}t_3) - e^{i(\vartheta_3-\vartheta_1)}\sin(\Omega_{0,0}t_1)\cos(\Omega_{0,1}t_2)\sin(\Omega_{0,0}t_3), \\
1 = -e^{i(\vartheta_1-\vartheta_3)}\sin(\Omega_{0,0}t_1)\sin(\Omega_{0,0}t_3) + \cos(\Omega_{0,0}t_1)\cos(\Omega_{0,1}t_2)\cos(\Omega_{0,0}t_3), \\
1 = -ie^{-i\vartheta_3}\cos(\Omega_{1,0}t_1)\cos(\Omega_{0,1}t_2)\sin(\Omega_{1,0}t_3) - ie^{-i\vartheta_1}\sin(\Omega_{1,0}t_1)\cos(\Omega_{1,1}t_2)\cos(\Omega_{1,0}t_3), \\
1 = -ie^{i\vartheta_3}\cos(\Omega_{1,0}t_1)\cos(\Omega_{1,1}t_2)\sin(\Omega_{1,0}t_3) - ie^{i\vartheta_1}\sin(\Omega_{1,0}t_1)\cos(\Omega_{0,1}t_2)\cos(\Omega_{1,0}t_3).
\end{array}\right. \tag{51}$$

In the previous approaches, within the LD limit, for implementing quantum gate, the $k\pi$ pulses $k = 1, 2, 3, ...$ of the laser beams are usually applied to drive the ions. The relevant LD parameters should be set sufficiently small such that the LD approximation could be satisfied. Here, in order to realize the desirable quantum gate with arbitrarily LD parameters (i.e., beyond the LD limit), we assume that the durations of the applied laser beams could be arbitrarily set (instead of the so-called $k\pi$ in the previous approaches). Indeed, the desired quantum gate could be implemented for arbitrarily experimental LD parameters, as long as the durations t_N and initial phases ϑ_N of the applied three laser beams ($N = 1, 2, 3$) are accurately set such that Eq. (50) is satisfied.
For equation (50), there maybe exist many solutions for any selected LD parameter. However, the practical existence of decoherence imposes the limit that the total duration of the present three-step pulse should be shorter than the decoherence times of both the atomic and motional states. This implies that exact solutions to Eq. (50) do not exist for certain experimental LD parameters. Certainly, for these parameters approximative solutions to Eq. (50) still exist and the CNOT gate could be approximately generated. The fidelity F for such an approximated realization is defined as the minimum among the probability amplitudes: $\alpha_{11}^{(3)}$, $\alpha_{22}^{(3)}$, $\alpha_{34}^{(3)}$, and $\alpha_{43}^{(3)}$, i.e. (27),

η	$\Omega t_1 = \Omega t_3$	Ωt_2	F
0.17	192.01	673.50	0.9935
0.18	292.03	637.85	0.9984
0.20	1.6690	255.07	0.9935
0.25	1.7287	207.94	0.9986
0.30	9.0200	438.00	0.9998
0.31	31.000	552.89	1.0000
0.35	177.00	1107.0	1.0000
0.40	2.0260	170.07	0.9999
0.50	97.304	57.310	0.9975
0.60	61.710	75.480	1.0000
0.70	66.900	160.85	0.9969
0.75	175.99	665.98	0.9998
0.85	73.110	105.91	0.9985
0.90	12.400	460.43	0.9992
0.95	25.300	415.21	0.9973

Table 3. Parameters for generating high-fidelity CNOT gates with arbitrarily selected LD parameters from 0.17 to 0.95 (27). Here $\vartheta_1 = -\vartheta_3 = \pi/2$, and $t_1 = t_3$.

$$F = \min\left\{\alpha_{11}^{(3)}, \alpha_{22}^{(3)}, \alpha_{34}^{(3)}, \alpha_{43}^{(3)}\right\} \tag{52}$$

It has been shown that the lifetime of the atomic excited state $|e\rangle$ reaches 1 s and the coherence superposition of vibrational states $|0\rangle$ and $|1\rangle$ can be maintained for up to 1 ms (32; 33). These allow us to perform the required three-step sequential laser manipulations; e.g., for $\Omega/(2\pi) \approx$ 500 kHz and $\eta = 0.20$ (4) the total duration $t = t_1 + t_2 + t_3 \approx 0.08$ ms. Table 3 provides some numerical results for arbitrarily selected LD parameters (not limited within the LD regime requiring $\eta \ll 1$) from 0.17 to 0.95. Here, the durations of the applied laser beam pulses are defined by the parameters Ωt_i with $i = 1, 2, 3$. It is seen that the fidelities of implementing the desirable CNOT gate for these LD parameters are significantly high (all of them larger than 99%).

3.3 Simplified approaches for implementing quantum logic gates

In fact, the above approach (with three laser pulses) for generating CNOT gate can be simplified, by using only two laser pulses (28). With the sequential two operations 1) and 2), the system undergoes the following evolutions:

$$\begin{array}{ll} \text{Input state} & \text{Output state} \\ |0\rangle|g\rangle \longrightarrow |\psi_a^{(1)}\rangle \longrightarrow |\psi_a^{(2)}\rangle & \\ |0\rangle|e\rangle \longrightarrow |\psi_b^{(1)}\rangle \longrightarrow |\psi_b^{(2)}\rangle & \\ |1\rangle|g\rangle \longrightarrow |\psi_c^{(1)}\rangle \longrightarrow |\psi_c^{(2)}\rangle & \\ |1\rangle|e\rangle \longrightarrow |\psi_d^{(1)}\rangle \longrightarrow |\psi_d^{(2)}\rangle & \end{array} \tag{53}$$

If

$$\alpha_{11}^{(2)} = \alpha_{22}^{(2)} = \alpha_{33}^{(2)} = \alpha_{42}^{(2)} = 1, \tag{54}$$

i.e.,(see, APPENDIX A):

$$\begin{cases} 1=\cos(\Omega_{0,0}t_1), \\ 1=\cos(\Omega_{0,0}t_1)\cos(\Omega_{0,1}t_2), \\ 1=i^{-1}e^{-i\vartheta_1}\sin(\Omega_{1,0}t_1)\cos(\Omega_{1,1}t_2), \\ 1=i^{-1}e^{i\vartheta_1}\sin(\Omega_{1,0}t_1)\cos(\Omega_{0,1}t_2), \end{cases} \tag{55}$$

then $|\psi_a^{(2)}\rangle=|0\rangle|g\rangle$, $|\psi_b^{(2)}\rangle=|0\rangle|e\rangle$, $|\psi_c^{(2)}\rangle=|1\rangle|e\rangle$, and $|\psi_d^{(2)}\rangle=|1\rangle|g\rangle$. Thus, the desirable CNOT gate (45) is realized.
The above condition could be achieved by properly setting the relevant experimental parameters, t_1, t_2, ϑ_1, and η as

$$t_1=\frac{2p\pi}{\Omega_{0,0}}, t_2=\frac{2m\pi}{\Omega_{0,1}}, \theta_1=(-1)^{q+1}\frac{\pi}{2}, \tag{56}$$

with $p,q,m=1,2,3...$, and

$$\eta^2=1-\frac{q-0.5}{2p}=2-\frac{\sqrt{2}(n-0.5)}{m}, \tag{57}$$

with $n=1,2,3,....$ This means that the CNOT gate (45) could be implemented, since all the experimental parameters related above are accurately controllable. This implies that the required laser pulses for implementing a CNOT gate could be really reduced to two ones. Due to decoherence(i.e., the limit of durations t_1+t_2), the integers p,q,m,n could not take arbitrary large values to let (57) be satisfied exactly, although their approximated solutions

η	$t_1\Omega$	$t_2\Omega$	$\theta_1=\pm\frac{\pi}{2}$	F
0.18	689.6666	993.3470	+	0.9907
0.20	1525.600	1410.200	+	0.9958
0.22	1261.700	1463.000	+	0.9984
0.25	1504.000	1192.800	-	0.9978
0.28	457.4064	326.7189	+	0.9967
0.30	328.6193	438.1591	-	0.9993
0.38	351.1877	284.3625	+	0.9994
0.40	490.0675	170.1623	+	0.9975
0.44	304.5596	283.1649	-	0.9980
0.53	347.0706	190.9979	+	0.9970
0.57	443.4884	492.7649	+	0.9993
0.64	385.5613	481.9516	-	0.9967
0.68	316.7005	395.8756	-	0.9950
0.73	377.2728	292.1111	-	0.9953
0.80	276.8880	281.2143	-	0.9980
0.86	436.5392	486.4535	+	0.9999
0.90	471.0198	460.5527	-	0.9971
0.96	318.7519	394.2894	+	0.9969

Table 4. CNOT gates implemented with sufficiently high fidelities for arbitrarily selected parameters (28).

η	$t_1\Omega$	$\alpha_{11}^{(1)}=\alpha_{21}^{(1)}$	$\alpha_{12}^{(1)}=\alpha_{22}^{(1)}$	$\alpha_{31}^{(1)}=\alpha_{41}^{(1)}$	$\alpha_{32}^{(1)}=\alpha_{42}^{(1)}$
0.18	267.75	0.97520	-0.22135	-0.21954	0.97560
0.20	243.65	0.99948	0.03218	0.03193	0.99949
0.22	179.76	0.97284	-0.23146	-0.23053	0.97306
0.24	168.13	1.00000	0.00000	0.00000	1.00000
0.26	129.49	0.97165	-0.23640	-0.24006	0.97076
0.28	130.92	0.99376	0.11153	0.11041	0.99389
0.30	104.95	0.99505	-0.09935	-0.09778	0.99521
0.32	92.35	0.99374	-0.11172	-0.10790	0.99416
0.34	79.49	0.98271	-0.18517	-0.18852	0.98207
0.36	80.64	0.99586	0.09088	0.09407	0.99557
0.38	67.33	0.99541	-0.09572	-0.09377	0.99559
0.40	68.44	0.98505	0.17225	0.16794	0.98580
0.42	54.57	0.98859	-0.15063	-0.15383	0.98810
0.44	55.56	0.99646	0.08411	0.08530	0.99636
0.46	111.30	0.97957	-0.20111	-0.19843	0.98012
0.48	41.83	0.97796	-0.20881	-0.20607	0.97854
0.50	42.72	1.00000	0.00000	0.00000	1.00000
0.52	43.67	0.97497	0.22234	0.21915	0.97570
0.54	87.23	1.00000	0.00000	0.00000	1.00000
0.56	132.93	0.96361	0.26731	0.26592	0.96400
0.58	118.42	0.97544	-0.22027	-0.22025	0.97544
0.60	29.81	0.99320	-0.11640	-0.11358	0.99353

Table 5. CNOT gates implemented with high fidelities for arbitrarily selected parameters(from 0.18 to 0.60) (29).

are still exists. This implies that the desirable CNOT gate is approximately implemented with a fidelity $F < 1$. Similar to that of Sec. 3.2, here the fidelity F of implementing the desirable gate is defined as the minimum among the values of $\alpha_{11}^{(2)}$, $\alpha_{22}^{(2)}$, $\alpha_{33}^{(2)}$ and $\alpha_{42}^{(2)}$, i.e., $F=\min\{\alpha_{11}^{(2)},\alpha_{22}^{(2)},\alpha_{33}^{(2)},\alpha_{42}^{(2)}\}$.

In table 4, we present some experimental parameters arbitrarily selected to implement the expected CNOT gate (45), with sufficiently high fidelities $F > 99\%$. For example, we have $F = 99.58\%$ for the typical LD parameter $\eta = 0.2$. It is also seen from the table that the present proposal still works for certain large LD parameters, e.g., 0.90, 0.96, etc.. For the experimental parameters $\eta = 0.2$ and $\Omega/(2\pi) \approx 500$ kHz, the total duration $t_1 + t_2$ for this implementation is about 0.9 ms. By increasing the Rabi frequency Ω via enhancing the power of the applied laser beams, the durations can be further shorten, and thus the CNOT gates could be realized more efficiently.

In fact, a CNOT gate (*apart from certain phase factors*) (39) could be still realized by a single laser pulse. By setting $\vartheta_1 = \pi/2$ and

$$\cos(\Omega_{0,0}t_1) = \sin(\Omega_{1,0}t_1) = 1, \tag{58}$$

η	$t_1\Omega$	$\alpha_{11}^{(1)}=\alpha_{21}^{(1)}$	$\alpha_{12}^{(1)}=\alpha_{22}^{(1)}$	$\alpha_{31}^{(1)}=\alpha_{41}^{(1)}$	$\alpha_{32}^{(1)}=\alpha_{42}^{(1)}$
0.62	30.64	0.99720	0.07473	0.07201	0.99740
0.64	31.52	0.96241	0.27158	0.26906	0.96312
0.66	62.42	0.99952	-0.03096	-0.03027	0.99954
0.68	95.26	0.99509	0.09898	0.09985	0.99500
0.70	353.53	0.99224	0.12437	0.12458	0.99221
0.72	178.61	0.97983	-0.19981	-0.20082	0.97963
0.74	82.49	0.99876	-0.04974	-0.05286	0.99860
0.76	50.12	0.99715	-0.07548	-0.07608	0.99710
0.78	186.67	0.96719	-0.25406	-0.25835	0.96605
0.80	155.88	0.99888	0.04737	0.04576	0.99895
0.82	175.54	0.99258	-0.12162	-0.12311	0.99239
0.84	17.27	0.97693	-0.21356	-0.21395	0.97685
0.86	18.04	0.99867	-0.05149	-0.05191	0.99865
0.88	18.88	0.99205	0.12582	0.12453	0.99221
0.90	19.79	0.95031	0.31129	0.31157	0.95022
0.92	153.85	0.99324	0.11610	0.11507	0.99336
0.94	39.40	0.99517	0.09817	0.09647	0.99534
0.96	60.04	0.99627	0.08632	0.08611	0.99629
0.98	122.12	0.99709	0.07617	0.07482	0.99720

Table 6. CNOT gates implemented with high fidelities for arbitrarily selected parameters(from 0.62 to 0.98) (29).

the operation (46) can realize the following two-qubit quantum operation (see, APPENDIX A)

$$\begin{array}{l} |0\rangle|g\rangle \longrightarrow |0\rangle|g\rangle \\ |0\rangle|e\rangle \longrightarrow |0\rangle|e\rangle \\ |1\rangle|g\rangle \longrightarrow -|1\rangle|e\rangle \\ |1\rangle|e\rangle \longrightarrow |1\rangle|g\rangle \end{array} \tag{59}$$

which is equivalent to the standard CNOT gate (45) between the external and internal states of the ion, apart from the phase factors -1.
Obviously, the condition (58) can be satisfied by properly setting the relevant experimental parameters: t_1 and η, as

$$t_1=\frac{2n\pi}{\Omega_{0,0}}, \eta^2=1-\frac{m-\frac{3}{4}}{n},\ n,m=1,2,3...., \tag{60}$$

with n and m being arbitrary positive integers. Because of the practical existence of decoherence, as we discussed above, the duration of the present pulse should be shorter than the decoherence times of both the atomic and motional states of the ion. This limits that the integers n could not take arbitrary large values to let Eq. (60) be exactly satisfied.
In tables 5 and 6 we present some numerical results for setting proper experimental parameters Ωt_1 (all of them $\lesssim 0.1$ ms for the experimental Rabi frequency $\Omega/(2\pi)\approx$ 500 KHz), to implement quantum operation (59) for the arbitrarily selected LD parameters (not limited within the LD regime requiring $\eta \ll 1$) from 0.18 to 0.98. It is seen that, the

probability amplitudes $\alpha_{11}^{(1)} = \alpha_{21}^{(1)}$ and $\alpha_{32}^{(1)} = \alpha_{42}^{(1)}$ are desirably large, most of them could reach to 0.99. While, unwanted probability amplitudes $\alpha_{12}^{(1)} = \alpha_{22}^{(1)}$ and $\alpha_{31}^{(1)} = \alpha_{41}^{(1)}$ are really significantly small; all of them is less than 0.32. This implies that the lowest fidelity $F = \min\{\alpha_{11}^{(1)}, \alpha_{21}^{(1)}, \alpha_{32}^{(1)}, \alpha_{42}^{(1)}\}$ for implementing the quantum operation (59) is larger than 95%.
Certainly, the above approximated solutions could be further improved by either relaxing the limit from the decoherence time or increasing Rabi frequency Ω (via increasing the powers of the applied laser beams) to shorten the operational time. Designing the applied laser pulse with so short duration is not a great difficulty for the current experimental technology, e.g., the femto-second (10^{-15}s) laser technique. Also, our numerical calculations show that the influence of the possibly-existing fluctuations of the applied durations is really weak. For example, for the Rabi frequency $\Omega/(2\pi) \approx 500$ kHz, the fluctuation $\delta t \approx 0.1\,\mu$s of the duration lowers the desirable probability amplitudes, i.e., $\alpha_{11}^{(1)}$ and $\alpha_{32}^{(1)}$ presented in tables 5 and 6, just about 5%. Thus, even consider the imprecision of the durations, the amplitude of the desirable elements, $\alpha_{11}^{(1)}$ and $\alpha_{32}^{(1)}$, are still sufficiently large, e.g., up to about 0.95. Therefore, the approach proposed here to implement the desirable quantum operation (59) for arbitrary LD parameters should be experimentally feasible.
Finally, we consider how to generate the standard CNOT gate (45) from the quantum operation (59) produced above. This could be achieved by just eliminating the unwanted phase factors in (59) via introducing another off-resonant laser pulse (10). Indeed, a first blue-sideband pulse (of frequency $\omega_L = \omega_{ea} + \nu$ and initial phase ϑ_2) induces the following evolution

$$|1\rangle|e\rangle \longrightarrow \cos(\Omega_{0,1}t_2)|1\rangle|e\rangle - e^{i\vartheta_2}\sin(\Omega_{0,1}t_2)|0\rangle|a\rangle, \tag{61}$$

but does not evolve the states $|0\rangle|g\rangle$, $|1\rangle|g\rangle$ and $|0\rangle|e\rangle$. Above, $|a\rangle$ is an auxiliary atomic level, and ω_{ea} being the transition frequency between it and the excited state $|e\rangle$. Obviously, a "π-pulse" defined by $\Omega_{0,1}t_2 = \pi$ generates a so-called controlled-Z logic operation (10)

$$\begin{array}{l} |0\rangle|g\rangle \longrightarrow |0\rangle|g\rangle \\ |0\rangle|e\rangle \longrightarrow |0\rangle|e\rangle \\ |1\rangle|g\rangle \longrightarrow |1\rangle|g\rangle \\ |1\rangle|e\rangle \longrightarrow -|1\rangle|e\rangle \end{array} \tag{62}$$

For the LD parameters from 0.18 to 0.98, and $\Omega/(2\pi) \approx 500$ kHz, the durations for this implementation are numerically estimated as $3.3 \times 10^{-3} \sim 1.2 \times 10^{-2}$ ms. Therefore, the standard CNOT gate (45) with a single trapped ion could be implemented by only two sequential operations demonstrated above.

4. Conclusions

In this chapter, we have summarized our works on designing properly laser pulses for preparing typical motional quantum states and implementing quantum logic gates with single trapped ions beyond the LD approximation. To generate the typical vibrational states (e.g., the coherence states, squeezed coherent states, odd/even coherent states and squeezed states) and implement CNOT gates of a single trapped ion, serval sequential laser pules are proposed to be applied to the trapped ion. It is shown that by properly set the frequency, duration, and phase, etc., of the each laser pulse the desired vibrational states and CNOT gates of a single trapped ion could be well generated with high fidelities.

5. APPENDIX A:

$$\begin{aligned}
\alpha_{11}^{(1)} &= \alpha_{21}^{(1)} = \cos(\Omega_{0,0}t_1) \\
\alpha_{12}^{(1)} &= i^{-1}e^{-i\vartheta_1}\sin(\Omega_{0,0}t_1) \\
\alpha_{22}^{(1)} &= i^{-1}e^{i\vartheta_1}\sin(\Omega_{0,0}t_1) \\
\alpha_{31}^{(1)} &= \alpha_{41}^{(1)} = \cos(\Omega_{1,0}t_1) \\
\alpha_{32}^{(1)} &= i^{-1}e^{-i\vartheta_1}\sin(\Omega_{1,0}t_1) \\
\alpha_{42}^{(1)} &= i^{-1}e^{i\vartheta_1}\sin(\Omega_{1,0}t_1)
\end{aligned} \tag{63}$$

$$\begin{aligned}
\alpha_{11}^{(2)} &= \cos(\Omega_{0,0}t_1) \\
\alpha_{12}^{(2)} &= i^{-1}e^{-i\vartheta_1}\sin(\Omega_{0,0}t_1)\cos(\Omega_{0,1}t_2) \\
\alpha_{13}^{(2)} &= -i^{-1}e^{i(\vartheta_2-\vartheta_1)}\sin(\Omega_{0,0}t_1)\sin(\Omega_{0,1}t_2) \\
\alpha_{21}^{(2)} &= i^{-1}e^{i\vartheta_1}\sin(\Omega_{0,0}t_1) \\
\alpha_{22}^{(2)} &= \cos(\Omega_{0,0}t_1)\cos(\Omega_{0,1}t_2) \\
\alpha_{23}^{(2)} &= -e^{-i\vartheta_2}\cos(\Omega_{0,0}t_1)\sin(\Omega_{0,1}t_2)
\end{aligned} \tag{64}$$

$$\begin{aligned}
\alpha_{31}^{(2)} &= e^{-i\vartheta_2}\cos(\Omega_{1,0}t_1)\sin(\Omega_{0,1}t_2) \\
\alpha_{32}^{(2)} &= \cos(\Omega_{1,0}t_1)\cos(\Omega_{0,1}t_2) \\
\alpha_{33}^{(2)} &= i^{-1}e^{-i\vartheta_1}\sin(\Omega_{1,0}t_1)\cos(\Omega_{1,1}t_2) \\
\alpha_{34}^{(2)} &= -i^{-1}e^{i(\vartheta_2-\vartheta_1)}\sin(\Omega_{1,0}t_1)\sin(\Omega_{1,1}t_2)
\end{aligned} \tag{65}$$

$$\begin{aligned}
\alpha_{41}^{(2)} &= i^{-1}e^{i(\vartheta_1-\vartheta_2)}\sin(\Omega_{1,0}t_1)\sin(\Omega_{0,1}t_2) \\
\alpha_{42}^{(2)} &= i^{-1}e^{i\vartheta_1}\sin(\Omega_{1,0}t_1)\cos(\Omega_{0,1}t_2) \\
\alpha_{43}^{(2)} &= \cos(\Omega_{1,0}t_1)\cos(\Omega_{1,1}t_2) \\
\alpha_{44}^{(2)} &= -e^{i\vartheta_2}\cos(\Omega_{1,0}t_1)\sin(\Omega_{1,1}t_2)
\end{aligned} \tag{66}$$

$$\begin{aligned}
\alpha_{11}^{(3)} &= \cos(\Omega_{0,0}t_1)\cos(\Omega_{0,0}t_3) - e^{i(\vartheta_3-\vartheta_1)}\sin(\Omega_{0,0}t_1)\cos(\Omega_{0,1}t_2)\sin(\Omega_{0,0}t_3) \\
\alpha_{12}^{(3)} &= -ie^{-i\vartheta_3}\cos(\Omega_{0,0}t_1)\sin(\Omega_{0,0}t_3) - ie^{-i\vartheta_1}\sin(\Omega_{0,0}t_1)\cos(\Omega_{0,1}t_2)\cos(\Omega_{0,0}t_3) \\
\alpha_{13}^{(3)} &= ie^{i(\vartheta_2-\vartheta_1)}\sin(\Omega_{0,0}t_1)\sin(\Omega_{0,1}t_2)\cos(\Omega_{0,1}t_3) \\
\alpha_{14}^{(3)} &= ie^{i(\vartheta_2-\vartheta_1-\vartheta_3)}\sin(\Omega_{0,0}t_1)\sin(\Omega_{0,1}t_2)\sin(\Omega_{0,1}t_3)
\end{aligned} \tag{67}$$

$$\begin{aligned}
\alpha_{21}^{(3)} &= -ie^{i\vartheta_1}\sin(\Omega_{0,0}t_1)\cos(\Omega_{0,0}t_3) - ie^{i\vartheta_3}\cos(\Omega_{0,0}t_1)\cos(\Omega_{0,1}t_2)\sin(\Omega_{0,0}t_3) \\
\alpha_{22}^{(3)} &= -e^{i(\vartheta_1-\vartheta_3)}\sin(\Omega_{0,0}t_1)\sin(\Omega_{0,0}t_3) + \cos(\Omega_{0,0}t_1)\cos(\Omega_{0,1}t_2)\cos(\Omega_{0,0}t_3) \\
\alpha_{23}^{(3)} &= -e^{i\vartheta_2}\cos(\Omega_{0,0}t_1)\sin(\Omega_{0,1}t_2)\cos(\Omega_{1,0}t_3) \\
\alpha_{24}^{(3)} &= -e^{i(\vartheta_2-\vartheta_3)}\cos(\Omega_{0,0}t_1)\sin(\Omega_{0,1}t_2)\sin(\Omega_{1,0}t_3)
\end{aligned} \tag{68}$$

$$\begin{aligned}
\alpha_{31}^{(3)} &= -ie^{i(\vartheta_3-\vartheta_2)}\cos(\Omega_{1,0}t_1)\sin(\Omega_{0,1}t_2)\sin(\Omega_{0,0}t_3) \\
\alpha_{32}^{(3)} &= e^{-i\vartheta_2}\cos(\Omega_{1,0}t_1)\sin(\Omega_{0,1}t_2)\cos(\Omega_{0,0}t_3) \\
\alpha_{33}^{(3)} &= \cos(\Omega_{1,0}t_1)\cos(\Omega_{0,1}t_2)\cos(\Omega_{1,0}t_3) - e^{i(\vartheta_3-\vartheta_1)}\sin(\Omega_{1,0}t_1)\cos(\Omega_{1,1}t_2)\sin(\Omega_{1,0}t_3) \\
\alpha_{34}^{(3)} &= -ie^{-i\vartheta_3}\cos(\Omega_{1,0}t_1)\cos(\Omega_{0,1}t_2)\sin(\Omega_{1,0}t_3) - ie^{-i\vartheta_1}\sin(\Omega_{1,0}t_1)\cos(\Omega_{1,1}t_2)\cos(\Omega_{1,0}t_3) \\
\alpha_{35}^{(3)} &= ie^{i(\vartheta_2-\vartheta_1)}\sin(\Omega_{1,0}t_1)\sin(\Omega_{1,1}t_2)\cos(\Omega_{2,0}t_3) \\
\alpha_{36}^{(3)} &= e^{i(\vartheta_2-\vartheta_1-\vartheta_3)}\sin(\Omega_{1,0}t_1)\sin(\Omega_{1,1}t_2)\sin(\Omega_{2,0}t_3)
\end{aligned} \tag{69}$$

$$\begin{aligned}
\alpha_{41}^{(3)} &= -e^{i(\vartheta_1-\vartheta_2+\vartheta_3)}\sin(\Omega_{1,0}t_1)\sin(\Omega_{0,1}t_2)\sin(\Omega_{0,0}t_3) \\
\alpha_{42}^{(3)} &= -ie^{i(\vartheta_1-\vartheta_2)}\sin(\Omega_{1,0}t_1)\sin(\Omega_{0,1}t_2)\cos(\Omega_{0,0}t_3) \\
\alpha_{43}^{(3)} &= -ie^{i\vartheta_3}\cos(\Omega_{1,0}t_1)\cos(\Omega_{1,1}t_2)\sin(\Omega_{1,0}t_3) - ie^{i\vartheta_1}\sin(\Omega_{1,0}t_1)\cos(\Omega_{0,1}t_2)\cos(\Omega_{1,0}t_3)
\end{aligned}$$

$$\alpha_{44}^{(3)} = \cos(\Omega_{1,0}t_1)\cos(\Omega_{1,1}t_2)\cos(\Omega_{1,0}t_3) - e^{i(\vartheta_1-\vartheta_3)}\sin(\Omega_{1,0}t_1)\cos(\Omega_{0,1}t_2)\sin(\Omega_{1,0}t_3)$$

$$\alpha_{45}^{(3)} = -ie^{i\vartheta_2}\cos(\Omega_{1,0}t_1)\sin(\Omega_{1,1}t_2)\cos(\Omega_{2,0}t_3)$$

$$\alpha_{46}^{(3)} = ie^{i(\vartheta_2-\vartheta_3)}\cos(\Omega_{1,0}t_1)\sin(\Omega_{1,1}t_2)\sin(\Omega_{2,0}t_3) \tag{70}$$

6. References

[1] W. Paul, *Rev. Mod. Phys.* 62, 531 (1990).
[2] D. J. Wineland, C. Monroe, W. M. Itano, D. Leibfried, B. E. King, and D. M. Meekhof, *J. Res. Natl. Inst. Stand. Technol.* 103, 259 (1998).
[3] D. Leibfried, R. Blatt, C. Monroe, and D. Wineland, *Rev. Mod. Phys.* 75, 281 (2003).
[4] D.M. Meekhof, C. Monroe, B.E. King, W.M. Itano and D.J. Wineland, *Phys. Rev. Lett.* 76, 1796 (1996).
[5] D. Leibfried, D. M. Meekhof, B. E. King, C. R. Monroe, W. M. Itano, and D. J. Wineland, *Phys. Rev. Lett.* 77, 4281 (1996).
[6] D. Leibfried, D. M. Meekhof, B. E. King, C. R. Monroe, W. M. Itano, and D. J. Wineland, *Phys. Rev. Lett.* 89, 247901 (2002).
[7] R. L. de Matos Filho and W. Vogel, *Phys. Rev. Lett.* 76, 608 (1996).
[8] J. I. Cirac, and P. Zoller, *Phys. Rev. Lett.* 74, 4091 (1995).
[9] K. Mølmer and A. Sørensen, *Phys. Rev. Lett.* 82, 1835 (1999).
[10] C. Monroe, D.M. Meekhof, B.E. King, W.M. Itano and D.J. Wineland, *Phys. Rev. Lett.* 75, 4714 (1995).
[11] C. A. Sackett, D. Kielpinski, B. E. King, C. Langer, V. Meyer, C. J. Myatt, M. Rowe, Q. A. Turchette, W. M. Itano, D. J. Wineland, and C. Monroe, *Nature (London)* 404, 256 (2000).
[12] F. Schmidt-Kaler, H. Häffner, M. Riebe, S. Gulde, G.P.T. Lancaster, T. Deuschle, C. Becher, C.F. Roos, J. Eschner, and R. Blatt, *Nature (London)* 422, 408 (2003).
[13] D. Leibfried, E. Knill, S. Seidelin, J. Britton, R. B. Blakestad, J. Chiaverini, D. B. Hume, W. M. Itano, J. D. Jost, C. Langer, R. Ozeri, R. Reichle, and D. J. Wineland, *Nature (London)* 438, 639 (2005).
[14] H. Häffner, W. Hänsel, C. F. Roos, J. Benhelm, D. Chek-al-kar, M. Chwalla, T. Körber, U. D. Rapol, M. Riebe, P. O. Schmidt, C. Becher, O. Ghühne, W. Dür, and R. Blatt, *Nature (London)* 438, 643 (2005).
[15] J. M. Raimond, M. Brune, and S. Haroche, *Rev. Mod. Phys.* 73, 565 (2001).
[16] Y. Makhlin, G. Schön, and A. Shnirman, *Rev. Mod. Phys.* 73, 357 (2001).
[17] N. A. Gershenfeld and I. L. Chuang, *Science* 275, 350 (1997).
[18] D. Loss and D. P. DiVincenzo, *Phys. Rev. A* 57, 120 (1998).
[19] W. Vogel and R. L. de Matos Filho, *Phys. Rev. A* 52, 4214 (1995).
[20] D. Stevens, J. Brochard, and A. M. Steane, *Phys. Rev. A* 58, 2750 (1998).
[21] A. Steane, *Appl. Phys. B: Lasers Opt.* B64, 623 (1997).
[22] G. Morigi, J. I. Cirac, M. Lewenstein, and P. Zoller, *Europhys. Lett.* 39, 13 (1997).
[23] L. F. Wei, Y.X. Liu and F. Nori, *Phys. Rev. A* 70, 063801 (2004).
[24] Q. Y. Yang, L. F. Wei, and L. E. Ding, *J. Opt.* B7, 5 (2005).
[25] M. Zhang, H. Y. Jia, X. H. Ji, K. Si, and L. F. Wei, *Acta Phys. Sin.*, 57, 7650 (2008).
[26] L. F. Wei, S.Y. Liu and X.L. Lei, *Phys. Rev. A* 65, 062316 (2002).

[27] L. F. Wei, M. Zhang, H.Y. Jia, and Y. Zhao, *Phys. Rev. A* 78, 014306 (2008).
[28] M. Zhang, X. H. Ji, H. Y. Jia, and L. F. Wei, *J. Phys.* B42, 035501 (2009).
[29] M. Zhang, H. Y. Jia, and L. F. Wei, *Opt. Communications.* 282, 1948 (2009).
[30] H. J. Lan, M. Zhang, and L. F. Wei, *Chin. Phys. Lett.* 27, 010304 (2010).
[31] M. Zhang, *"quantum-state manipulation with trapped ions and electrons on the liquid Helium"*, Southwest Jiaotong University Doctor Degree Dissertation, 2010.
[32] P. A. Barton, C. J. S. Donald, D. M. Lucas, D. A. Stevens, A. M. Steane and D. N. Stacey, *Phys. Rev. A* 62, 032503 (2000).
[33] Ch. Roos, Th. Zeiger, H. Rohde, H. C. Näerl, J. Eschner, D. Leibfried, F. Schmidt-Kaler, and R. Blatt, *Phys. Rev. Lett.* 83, 4713 (1999).
[34] P. Shor, in Proceedings of the 35th Annual Symposium on the Foundations of Computer Science, edited by Shafi Goldwasser (IEEE Computer Society Press, New York, 1994), p. 124.
[35] L. K. Grover, *Phys. Rev. Lett.* 79, 325 (1997).
[36] T. Sleator and H. Weinfurter, *Phys. Rev. Lett.* 74, 4087 (1995).
[37] D. P. DiVincenzo, *Phys. Rev. A* 51, 1015 (1995).
[38] A. Barenco, D. Deutsch, A. Ekert, and R. Jozsa, *Phys. Rev. Lett.* 74, 4083 (1995).
[39] C. Monroe, D. Leibfried, B.E. King, D.M. Meekhof, W.M. Itano, and D.J. Wineland, *Phys. Rev. A* 55, R2489 (1997).

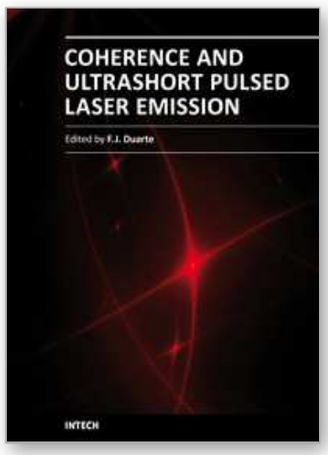

Coherence and Ultrashort Pulse Laser Emission

Edited by Dr. F. J. Duarte

ISBN 978-953-307-242-5
Hard cover, 688 pages
Publisher InTech
Published online 30, November, 2010
Published in print edition November, 2010

In this volume, recent contributions on coherence provide a useful perspective on the diversity of various coherent sources of emission and coherent related phenomena of current interest. These papers provide a preamble for a larger collection of contributions on ultrashort pulse laser generation and ultrashort pulse laser phenomena. Papers on ultrashort pulse phenomena include works on few cycle pulses, high-power generation, propagation in various media, to various applications of current interest. Undoubtedly, Coherence and Ultrashort Pulse Emission offers a rich and practical perspective on this rapidly evolving field.

InTech Europe
University Campus STeP Ri
Slavka Krautzeka 83/A
51000 Rijeka, Croatia
Phone: +385 (51) 770 447
Fax: +385 (51) 686 166
www.intechopen.com

InTech China
Unit 405, Office Block, Hotel Equatorial Shanghai
No.65, Yan An Road (West), Shanghai, 200040, China
中国上海市延安西路65号上海国际贵都大饭店办公楼405单元
Phone: +86-21-62489820
Fax: +86-21-62489821

IntechOpen